Communications in Mathematics and Applications
Vol. 14, No. 2, pp. 685–705, 2023
ISSN 0975-8607 (online); 0976-5905 (print)
Published by RGN Publications
DOI: 10.26713/cma.v14i2.1899

http://www.rgnpublications.com

Research Article

Non-Newtonian Eyring-Powell-Casson Nanofluid Flow via Porous Medium: Numerical Analysis

D. Hymavathi

Department of Mathematics, University College of Science, Mahatma Gandhi University, Yellareddygudem, Nalgonda 508254, Telangana, India
hymavathi@mguniversity.ac.in

Received: May 6, 2022 **Accepted:** November 11, 2022

Abstract. Investigations have been conducted in this paper by considering the combined convective Eyring-Powell Casson nanofluid through porous media with thermal radiation and chemical reaction. The possible comparability transformations are used to present a flow problem in a non-linear system of ordinary differential equations with the assistance of Keller-Box method, known as implicit finite difference scheme, where the important conclusions have been drawn and discussed in the form of graphs and through the validation of the numerical outcomes for the various values of flow parameters like thermophoresis parameter, viscous dissipation, thermal radiation, porosity, Brownian motion parameter, and fluid parameters.

Keywords. Eyring-Powell fluids, Porous medium, Casson nanofluid, Mixed convection, Viscous dissipation, Chemical reaction

Mathematics Subject Classification (2020). 32G34, 34B07, 80A19, 74F05

1. Introduction

Electro-conductive polymer material properties in modern smart technologies such as the aerospace and naval industries. The discrepancy between the nonlinear relations of shear rate and shear stress is what defines a non-Newtonian fluid. Non-Newtonian fluids have a wide range of applications in science. Printing colours, greases, blood, inks, toothpaste, greasing oils, shampoos, cosmetics, nail polish, creams, lotions, shaving suds, and munchies are all examples of non-Newtonian fluids (see, Attia [5], Keimanesh *et al*. [22], Shojaeian and Koşar [38], Rehman

et al. [36], and Yilmaz *et al*. [41]). Non-Newtonian and Newtonian fluids are the two primary types of fluids. Non-Newtonian types are studied in many modern engineering applications. Petroleum drilling muds, biological gels, polymer synthesis, and food processing are just a few of the industries that use non-Newtonian fluids. On the other hand non-Newtonian fluids with shear self-governing viscosity, on the other hand, nonetheless show typical stress differences and non-Newtonian behaviour. Many salt solutions as well as many different liquids encountered in research and technology, such as detergents, dental creams, and physiological fluids are non-Newtonian fluids. Furthermore, it can be used in conjunction with magnetohydrodynamics (see, Eldabe and Sallam [11], Eldabe *et al*. [12], and Hameed and Nadeem [15]). A colloidal deferment containing nano particles in a base fluid is referred to as a nanofluid. Because of the unique qualities of nanofluids, it is necessary to investigate technical applications ranging from being utilised in the automobile industry and in the medical profession, and in power plant cooling systems. To name a few, heat transfer applications (as in geothermal energy extraction, smart fluids, and nuclear reactors). And automotive applications (as nanofluid coolant and nanofluid in fuel, brakes, and other), when compared to base fluids, nanofluids have improved physical characteristics such as conductive heat transfer coefficients, thermal diffusivity, mass diffusivity, viscosity, and connectivity. Casson's fluid model was originally introduced in 1959. Casson fluid has yield stress, which alters flow behavior. Casson fluid is a kind of fluid independent of stress with constant viscosity known as non-Newtonian fluid. With an infinite viscosity at a zero stress rate, but when shear stress is increased to an unlimited level, the viscosity becomes zero for the Casson fluid. Because of its elements such as red cells, plasma, protein, and so on, this fluid model is also recommended for the investigation of human blood. Casson fluids include blood, stuffs, honey, jelly, slurries, soups, artificial fibres and so on. Ahmad *et al*. [3] presents Casson nanofluid along with Newtonian heating. Sarojamma and Vendabai [37] examined the results of Casson nanofluid passing through a perpendicular cylinder with the effect of a crossways magnetic field, which resulted in intramural heat production or absorption. Krishnendu *et al*. [26] investigated non-Newtonian Casson fluid flow across the stretched decreasing with magnetohydrodynamics and mass transfer at wall in great detail. Hussanan *et al*. [19] study the Casson non-Newtonian fluid in an unstable heat exchange flow with Newtonian heating over a perpendicular oscillating plate. Hussanan *et al*. [18] have investigated the MHD Casson fluid heat transfer and Newtonian heating. Malik *et al*. [30] utilised the Keller box scheme to explore the Cattaneo-Christov Casson nanofluid heat flux model with a variable viscosity and magnetic field influence. Raju *et al*. [34] investigated the thermal and solute transfer characteristics of the flow of Casson fluid across an exponentially permeable stretched surface, as well as the impacts of magnetic field, viscous dissipation, heat radiation, and chemical reaction. Hayat *et al*. [16] investigated an impact of Dufour and Soreton the 2-D flow of a non-Newtonian Casson fluid produced by the stretching of an electrically conducting flat surface, and they used the homotopy analysis approach to intervene and fix the difficulties. Abolbashari *et al*. [1] conducted an analytical study of the fluid flow, thermal, and mass transfer of non-Newtonian Casson nanofluid over the stretched convective surface boundary conditions. Hussain *et al*. [17] investigated an impact of convective thermal, solute circumstances with viscous dissipation on Casson nanofluid flow. Thermal radiation has a significant influence on industry, particularly in the assembly of industrial equipment such as rockets, gas turbines, satellites, nuclear power

plants, space vehicles, and many others. Thermal radiation is about the transmission of energy, emphasising the need for a better knowledge of radiative transfer in these processes. Dognchi and Ganji [9] investigated the influence of thermal radiation on nanofluid flow and heat transfer. Ramesh *et al*. [35] offered a mathematical study of Casson fluid that took heat radiation into consideration. Pramanik [32] investigated the combined impact of suction/blowing and heat radiation in a Casson fluid boundary layer flow over an exponentially extending sheet. Chemical reaction studies involving heat transfer have major applications in technology and industry. Chemical reactions occur in a variety of industrial applications, including the manufacture of ceramics or glassware, polymer synthesis, food processing, and so on, as a result of a chemical interaction between a foreign material and a fluid Stretching the sheet under different physical circumstances causes the velocity ratio, momentum slip, and magnetic parameters to rise, causing the velocity boundary layer thickness to decrease, and they investigated the influence of chemical reactions on mass and heat transfer. MHD boundary layer flow with viscous dissipation, thermal radiation, mixed convection, and other phenomena, previous stretched sheet and discovered that as the magnetic field rose, so did the Nusselt number, skin friction coefficient, and Sherwood number (see, Kumar and Gangadhar [27], El-Aziz and Afify [10], Krishnamurthy *et al*. [25], Mabood *et al*. [28], and Ibrahim *et al*. [20]). Non-Newtonian fluids, unlike viscous fluids, frequently do not define the flow pattern using Navier-Stokes equations because the fluids include a highly nonlinear relationship between stress and strain. Various theoretical models, such as Power law fluids, Maxwell fluids, Micropolar fluids, Jeffery fluid, Williamson fluid, and Giesekus fluid, are proposed to represent the behavior of non-Newtonian fluids. Furthermore, the Eyring-Powell fluid model is one of the fluid models that displays non-Newtonian behaviour.For primarily two reasons, the Eyring-Powell fluid model is preferred over other non-Newtonian fluid models: the kinetic theory of liquids is used to develop the concept rather than empirical relationships as seen in the power-law fluids model, and (i) the kinetic theory of liquids is used to develop the concept rather than empirical relationships as seen in the power-law fluids model. (ii) the behaviour of Newtonian and non-Newtonian fluids at high and intermediate shear rates The Eyring-Powell model has various applications in science and technology, including engineering processes, chemical and polymer synthesis, and so on (Fatunmbi [13]) used the *Finite Element Method* (FDM) to get the numerical solution of an Eyring-Powell fluid. Nazeer *et al*. [31] investigated Eyring-Powell fluid. FEM is used to numerically test the nanofluid flow. Javed *et al*. [21] use the Keller-Box technique to provide an approximate solution for an unsteady flow of Eyring-Powell fluid under magnetic influences. Rahimi *et al*. [33] created a numerical collocation technique approach to address the nonlinear flow issue across a stretched sheet. They discovered that the Eyring-Powell inertial parameter causes the velocity distribution to accelerate. Khan *et al*. [24] introduce the concept of Eyring-Powell fluid cross flow with entropy production. The HAM and Runge-Kutta techniques were used to arrive at the answer. The perturbation theory was employed by Ahmad *et al*. [2] to describe the flow of an Eyring-Powell fluid via a circular conduit. Malik *et al*. [29] investigated the Eyring-Powell fluid in mixed convection flow. Chamkha *et al*. [8] discussed the uniform wall heat flux and uniform wall temperature cases in which the Nusselt number, Sherwood number, and skin friction parameters decreased in the presents of magnetic field and porous medium increased due to imposition of fluid suction at the surface. Chamkha [6] investigated

the effects of Joule heating and viscous dissipation discussed for three types of thermal boundary conditions namely isoflux-isothermal, isothermal-isothermal, and isothermal-isoflux for the Channe's left-right walls. Takhar *et al*. [39] investigated the magnetic field, free stream velocity and hall current characteristics of a rotating fluid layer flow over a moving plate. Impact of mixed convection of fully developed polar fluid in a vertical channel has carried out by Chamkha *et al*. [7]. Heat transfer characteristics of unsteady oscillators two viscous immiscible fluids has been discussed via a horizontal channel by Umavathi *et al*. [40]. in their study Al-Mudhaf *et al*. [4] numerically investigated the effects of Marangoni convection flow for MHD thermosolutal in terms of heat generation and absorption. By employing finite-difference method a fluid layer analysis is discussed for mixed convective nanofluid in a porous medium by Gorla *et al*. [14].

According to the findings of the preceding research, transport in porous medium flows is critical in fuel cell technologies, geothermics, materials processing, trickling bed chromatography, and other fields. Many of these applications include coupled heat and mass transport in free convection boundary layer flows in porous media. The study of Casson fluid flow in a porous medium is becoming increasingly important in modern technology and science, such as petroleum drilling, polymer engineering, specific separation processes, food and paper production, and other industrial operations.In this work, the flow of Casson nanofluid toward a stretched porous surface with viscous dissipation, heat radiation, and chemical reaction must be investigated.

2. Mathematical Flow Model of the Problem

$$\frac{\partial u}{\partial x}+\frac{\partial v}{\partial y}=0, \tag{2.1}$$

$$u\frac{\partial u}{\partial x}+v\frac{\partial u}{\partial y}=\left(v+\frac{1}{\rho\beta c}\right)\left(\frac{\partial^2 u}{\partial x^2}+\frac{\partial^2 u}{\partial y^2}\right)-\frac{1}{3\rho\delta^* c^3}\frac{\partial}{\partial x}\left\{2\left(\frac{\partial u}{\partial x}\right)^2+2\left(\frac{\partial v}{\partial y}\right)^2+\left(\frac{\partial u}{\partial y}+\frac{\partial v}{\partial x}\right)^2\right\}\frac{\partial u}{\partial x}$$
$$-\frac{1}{6\rho\delta^* c^3}\frac{\partial}{\partial y}\left\{2\left(\frac{\partial u}{\partial x}\right)^2+2\left(\frac{\partial v}{\partial y}\right)^2+\left(\frac{\partial u}{\partial y}+\frac{\partial v}{\partial x}\right)^2\right\}\left(\frac{\partial u}{\partial y}+\frac{\partial v}{\partial x}\right)\pm\frac{g\beta_0(T-T_\infty)}{\rho}$$
$$\pm\frac{g\beta_1(C-C_\infty)}{\rho}-\frac{\mu}{k}u, \tag{2.2}$$

$$u\frac{\partial v}{\partial x}+v\frac{\partial v}{\partial y}=\left(v+\frac{1}{\rho\beta c}\right)\left(\frac{\partial^2 v}{\partial x^2}+\frac{\partial^2 v}{\partial y^2}\right)-\frac{1}{6\rho\delta^* c^3}\frac{\partial}{\partial x}\left\{2\left(\frac{\partial u}{\partial x}\right)^2+2\left(\frac{\partial v}{\partial y}\right)^2+\left(\frac{\partial u}{\partial y}+\frac{\partial v}{\partial x}\right)^2\right\}$$
$$\cdot\left(\frac{\partial u}{\partial y}+\frac{\partial v}{\partial x}\right)-\frac{1}{3\rho\delta^* c^3}\frac{\partial}{\partial y}\left\{2\left(\frac{\partial u}{\partial x}\right)^2+2\left(\frac{\partial v}{\partial y}\right)^2+\left(\frac{\partial u}{\partial y}+\frac{\partial v}{\partial x}\right)^2\right\}\frac{\partial v}{\partial y}$$
$$\pm\frac{g\beta_0(T-T_\infty)}{\rho}\pm\frac{g\beta_1(C-C_\infty)}{\rho}-\frac{\mu}{k}u, \tag{2.3}$$

$$u\frac{\partial T}{\partial x}+v\frac{\partial T}{\partial y}=\alpha\left(\frac{\partial^2 T}{\partial y^2}+\frac{\partial^2 T}{\partial x^2}\right)+\tau\left\{D_B\left(\frac{\partial T}{\partial x}\frac{\partial C}{\partial x}+\frac{\partial T}{\partial y}\frac{\partial C}{\partial y}\right)+\left(\frac{D_T}{T_\infty}\right)\left[\left(\frac{\partial T}{\partial x}\right)^2+\left(\frac{\partial T}{\partial y}\right)^2\right]\right\}$$
$$-\frac{1}{(\rho c)_f}\frac{\partial q_r}{\partial y}+\frac{\nu}{\rho c_p}\left[\left(\frac{\partial u}{\partial x}\right)^2+\left(\frac{\partial u}{\partial y}\right)^2\right], \tag{2.4}$$

$$u\frac{\partial C}{\partial x}+v\frac{\partial C}{\partial y}=D_B\left(\frac{\partial^2 C}{\partial x^2}+\frac{\partial^2 C}{\partial y^2}\right)+\frac{D_T}{T_\infty}\left(\frac{\partial^2 T}{\partial x^2}+\frac{\partial^2 T}{\partial y^2}\right)-k(C-C_\infty)-\gamma\phi\,. \tag{2.5}$$

Boundary conditions are $u = u_w(x) = ax$, $v = 0$, $-k\left(\frac{\partial T}{\partial x} + \frac{\partial T}{\partial y}\right) = h_f(T_f - T)$, $C = C_w$, at $y = 0$,

$$u \to u_\infty(x) = 0,\ v \to 0,\ T \to T_\infty, \quad C \to C_\infty \text{ as } y \to \infty, \tag{2.6}$$

$$\frac{\partial u}{\partial x} + \frac{\partial v}{\partial y} = 0, \tag{2.7}$$

$$u\frac{\partial u}{\partial x} + v\frac{\partial u}{\partial y} = \left(v + \frac{1}{\rho\beta c}\right)\frac{\partial^2 u}{\partial y^2} - \frac{1}{2\rho\delta^* c^3}\left(\frac{\partial u}{\partial y}\right)^2\frac{\partial^2 u}{\partial y^2} \pm \frac{g\beta_0(T - T_\infty)}{\rho} \pm \frac{g\beta_1(C - C_\infty)}{\rho} - \frac{\mu}{k}u, \tag{2.8}$$

$$u\frac{\partial T}{\partial x} + v\frac{\partial T}{\partial y} = \alpha\frac{\partial^2 T}{\partial y^2} + \tau\left\{D_B\left(\frac{\partial T}{\partial y}\frac{\partial C}{\partial y}\right) + \left(\frac{D_T}{T_\infty}\right)\left(\frac{\partial T}{\partial x}\right)^2\right\} - \frac{1}{(\rho c)_f}\frac{\partial q_r}{\partial y} + \frac{\nu}{\rho c_p}\left(\frac{\partial u}{\partial y}\right)^2, \tag{2.9}$$

$$u\frac{\partial C}{\partial x} + v\frac{\partial C}{\partial y} = D_B\frac{\partial^2 C}{\partial y^2} + \frac{D_T}{T_\infty}\left(\frac{\partial^2 T}{\partial y^2}\right) - k(C - C_\infty). \tag{2.10}$$

Boundary conditions are $u = u_w(x) = ax$, $v = 0$, $-k\frac{\partial T}{\partial y} = h_f(T_f - T)$, $C = C_w$, at $y = 0$,

$$u \to u_\infty(x) = 0,\ T \to T_\infty, \quad C \to C_\infty \text{ as } y \to \infty. \tag{2.11}$$

3. Similarity Transformation

$$\psi = (av)^{\frac{1}{2}}xf(\eta),\ \theta(\eta) = \frac{T - T_\infty}{T_w - T_\infty},\ \phi(\eta) = \frac{C - C_\infty}{C - C_\infty},\ \eta = \left(\frac{a}{v}\right)^{\frac{1}{2}}y, \tag{3.1}$$

$$(1+\omega)f''' + ff'' - f'^2 - \omega\lambda f''^2 f''' \pm \beta\theta \pm \delta\varphi + k_1 f' = 0, \tag{3.2}$$

$$\frac{1}{Pr}\left(1 + \frac{4}{3}N\right)\theta'' + f\theta' + Nb\,\phi'\theta' + Nt\,\theta'^2 + Ec(f'')^2 + Q\theta = 0, \tag{3.3}$$

$$\frac{1}{Pr}\phi'' + Le\,f\phi' + \frac{Nt}{Nb}\theta'' - K\phi = 0. \tag{3.4}$$

Boundary conditions $f(\eta) = 0$, $f'(\eta) = 1$,

$$\theta'(\eta) = -Bi(1 - \theta(\eta)),\ \ \phi(\eta) = 1 \ \text{ at } \eta = 0,$$

$$f'(\eta) \to 0,\ \ \theta(\eta) \to 0,\ \ \phi(\eta) \to 0 \ \text{ as } \eta \to \infty, \tag{3.5}$$

where

fluid parameters: $\omega = \frac{1}{\mu\delta^* c}$, $\lambda = \frac{a^3x^2}{2c^2v}$,

thermal buoyancy parameter: $\beta = \frac{g\beta_0(T_w - T_\infty)}{\rho a}$,

mass buoyancy parameter: $\delta = \frac{g\beta_1(C_w - C_\infty)}{\rho a}$,

Prandtl number (Pr): $\frac{v}{\alpha}$,

Lewis number (Le): $= \frac{\alpha}{D_B}$,

thermophoresis parameter: $Nt = \frac{\tau D_T(T_f - T_\infty)}{\nu T_\infty}$,

Brownian movement parameter: $Nb = \frac{\tau D_B(C_w - C_\infty)}{v}$,

Biot number: $Bi = \frac{h_f}{k}\left(\frac{v}{a}\right)^{\frac{1}{2}}$,

temperature absorption ($Q < 0$), Q temperature generation ($Q > 0$) parameter,

Nusselt number $= Nu_x$, Sherwood number $= Sh_x$ and skin-friction coefficient $= C_{fx}$,

$$C_{fx} = \frac{\tau_w}{\rho u_w^2}\tau_w = \left[\left(1+\frac{1}{\delta^* c}\right)\frac{\partial y}{\partial x} - \frac{1}{6\delta^* c^3}\left(\frac{\partial u}{\partial y}\right)^3\right] \text{ at } y = 0,$$

$$Nu_x = \frac{xq_w}{k(T_f - T_\infty)}q_w = -k\left[\frac{dT}{dy}\right]_{y=0},$$

$$Sh_x = \frac{xq_m}{D_B(C_w - C_\infty)}q_m = -D_B\left[\frac{\partial C}{\partial y}\right]_{y=0}.$$

By using the similarity transformations described below:

$$Re_x^{\frac{1}{2}}C_{fx} = \left[(1+\omega)f''(0) - \frac{\lambda}{3}f''^3(0)\right],$$

$$Re_x^{-\frac{1}{2}}Nu_x = -\theta'(0),$$

$$Re_x^{-\frac{1}{2}}S_{h_x} = -\phi'(0),$$

where $Re_x = \frac{xu_w}{\upsilon}$ is the Reynolds number.

4. Numerical Solution of the Problem

The Keller-Box technique (Keller [23]) is used to obtain the numerical solution to the modelled equations. Because of its quick convergence, this approach is chosen above many others. This system is intrinsically stable and convergent to the second order. Furthermore, it passes the Von Neumann stability test, which establishes the condition for the convergence of numerical solutions to the real solution of PDEs through the use of consistency and stability of numerical solutions. KBM is used to find the localised solution to equations (3.2)-(3.5). This is one of the most commonly used approaches for getting approximate solutions to the boundary layer issue. KBM has been frequently used to study laminar boundary layer flows, and its findings outperform other techniques. The Keller-Box technique is made up of the following steps:

- First, the controlling equations must be written into a first order system of equations.
- The domain is discretized after decreasing the order of equations, allowing us to calculate the estimated solution across each subdomain rather than the full domain. This produces more accurate findings.
- In order to get finite difference equations, central difference derivatives and the average of function midpoints are utilised.
- As Keller detailed, Newton's technique is next applied to linearize the resulting equations. And make a tridiagonal matrix out of them.
- Finally, the ultimate result is obtained by LU decomposition.

To apply the Keller-Box method, first construct the equations (3.2)-(3.5) as a system of first order differential equations with certain variables, and then solve the resulting equations:

$$f' = p, \tag{4.1}$$

$$f'' = p' = q, \tag{4.2}$$

$$\theta = g \Rightarrow g' = n, \tag{4.3}$$

$$\varphi = s \Rightarrow s' = t, \tag{4.4}$$

$$(1+\omega)q' + fq - p^2 - \omega\lambda q^2 q' \pm \beta g \pm \delta s + Kp = 0, \tag{4.5}$$

$$\frac{1}{Pr}\left(1+\frac{4}{3}N\right)n' + fn + Nb\,Sn + Nt\,n^2 + Ec(q)^2 + Qg = 0, \tag{4.6}$$

$$\frac{1}{Pr}t' + Le\,ft + \frac{Nt}{Nb}n' - Rs = 0. \tag{4.7}$$

The corresponding boundary conditions:

$$\begin{aligned} &f(\eta) = 0,\ p(\eta) = 1,\\ &n(\eta) = -Bi(1-g(\eta)),\ s(\eta) = 1,\ \text{ at }\ \eta = 0,\\ &p(\eta) \to 0,\ g(\eta) \to 0,\ s(\eta) \to 0,\quad \text{as }\ \eta \to \infty. \end{aligned} \tag{4.8}$$

The system of differential equations must be discretized after getting the first-order system in order to determine the estimated solution. Typically, discretization is accomplished by split the domain into a consistent grid. A smaller grid yields more precision in numerical calculations:

$$\eta_0 = 0,\ \ \eta_n = \eta_{n-1} + h,\ \ n = 1,2,3,\ldots,J-1,\ \ \eta_J = \eta_\infty. \tag{4.9}$$

In this issue, we have set $h = 0.001$. Then, using central differences, difference equations are produced. The mean averages of functions are used to replace them. The ordinary differential system (4.1)-(4.7) is then transformed into the nonlinear algebraic equations shown below:

$$\frac{f_j - f_{j-1}}{h_j} = \frac{p_j + p_{j-1}}{2}, \tag{4.10}$$

$$\frac{p_j - p_{j-1}}{h_j} = \frac{q_j + q_{j-1}}{2}, \tag{4.11}$$

$$\frac{g_j - g_{j-1}}{h_j} = \frac{n_j + n_{j-1}}{2}, \tag{4.12}$$

$$\frac{s_j - s_{j-1}}{h_j} = \frac{t_j + t_{j-1}}{2}, \tag{4.13}$$

$$\begin{aligned} &(1+\omega)\left(\frac{q_j - q_{j-1}}{h_j}\right) + \left(\frac{f_j + f_{j-1}}{2}\right)\left(\frac{q_j + q_{j-1}}{2}\right) - \left(\frac{p_j + p_{j-1}}{2}\right)^2 - \omega\lambda\left(\frac{q_j + q_{j-1}}{2}\right)^2\left(\frac{q_j - q_{j-1}}{h_j}\right)\\ &\quad \pm \beta\left(\frac{g_j + g_{j-1}}{2}\right) \pm \delta\left(\frac{s_j + s_{j-1}}{2}\right) + K\left(\frac{p_j + p_{j-1}}{2}\right) = 0, \end{aligned} \tag{4.14}$$

$$\begin{aligned} &\frac{1}{Pr}\left(1+\frac{4}{3}N\right)\left(\frac{n_j - n_{j-1}}{h_j}\right) + \left(\frac{f_j + f_{j-1}}{2}\right)\left(\frac{n_j + n_{j-1}}{2}\right) + Nb\left(\frac{t_j + t_{j-1}}{2}\right)\left(\frac{n_j + n_{j-1}}{2}\right)\\ &\quad + Nt\left(\frac{n_j + n_{j-1}}{2}\right)^2 + Ec\left(\frac{q_j + q_{j-1}}{2}\right)^2 + Q\left(\frac{g_j + g_{j-1}}{2}\right) = 0, \end{aligned} \tag{4.15}$$

$$\frac{1}{Pr}\left(\frac{t_j - t_{j-1}}{h_j}\right) + Le\left(\frac{f_j + f_{j-1}}{2}\right)\left(\frac{t_j + t_{j-1}}{2}\right) + \frac{Nt}{Nb}\left(\frac{n_j - n_{j-1}}{h_j}\right) - R\left(\frac{s_j + s_{j-1}}{2}\right) = 0. \tag{4.16}$$

The obtained equations by using Newton's method for above equations are then linearized the $(i+1)$th iterate can be written as

$$\left.\begin{aligned} &(f)_j^{(i+1)} = (f)_j^{(i)} + \delta(f)_j^{(i)},\quad (p)_j^{(i+1)} = (p)_j^{(i)} + \delta(p)_j^{(i)},\quad (q)_j^{(i+1)} = (q)_j^{(i)} + \delta(q)_j^{(i)},\\ &(g)_j^{(i+1)} = (g)_j^{(i)} + \delta(g)_j^{(i)},\quad (n)_j^{(i+1)} = (n)_j^{(i)} + \delta(n)_j^{(i)},\quad (s)_j^{(i+1)} = (s)_j^{(i)} + \delta(s)_j^{(i)},\\ &(t)_j^{(i+1)} = (t)_j^{(i)} + \delta(t)_j^{(i)}. \end{aligned}\right\} \tag{4.17}$$

The above terms substituted into the equations (4.10)-(4.16) and a linear tri-diagonal system is acquired as

$$\frac{((f)_j^{(i)}+\delta(f)_j^{(i)})-((f)_{j-1}^{(i)}+\delta(f)_{j-1}^{(i)})}{h_j}=\frac{((p)_j^{(i)}+\delta(p)_j^{(i)})+((p)_{j-1}^{(i)}+\delta(p)_{j-1}^{(i)})}{2}, \tag{4.18}$$

$$\frac{((p)_j^{(i)}+\delta(p)_j^{(i)})-((p)_{j-1}^{(i)}+\delta(p)_{j-1}^{(i)})}{h_j}=\frac{((q)_j^{(i)}+\delta(q)_j^{(i)})+((q)_{j-1}^{(i)}+\delta(q)_{j-1}^{(i)})}{2}, \tag{4.19}$$

$$\frac{((g)_j^{(i)}+\delta(g)_j^{(i)})-((g)_{j-1}^{(i)}+\delta(g)_{j-1}^{(i)})}{h_j}=\frac{((n)_j^{(i)}+\delta(n)_j^{(i)})+((n)_{j-1}^{(i)}+\delta(n)_{j-1}^{(i)})}{2}, \tag{4.20}$$

$$\frac{((s)_j^{(i)}+\delta(s)_j^{(i)})-((s)_{j-1}^{(i)}+\delta(s)_{j-1}^{(i)})}{h_j}=\frac{((t)_j^{(i)}+\delta(t)_j^{(i)})+((t)_{j-1}^{(i)}+\delta(t)_{j-1}^{(i)})}{2}, \tag{4.21}$$

$$\begin{aligned}
&(1+\omega)\left(\frac{((q)_j^{(i)}+\delta(q)_j^{(i)})-((q)_{j-1}^{(i)}+\delta(q)_{j-1}^{(i)})}{h_j}\right)+\left(\frac{((f)_j^{(i)}+\delta(f)_j^{(i)})+((f)_{j-1}^{(i)}+\delta(f)_{j-1}^{(i)})}{2}\right)\\
&\cdot\left(\frac{((q)_j^{(i)}+\delta(q)_j^{(i)})+((q)_{j-1}^{(i)}+\delta(q)_{j-1}^{(i)})}{2}\right)-\left(\frac{((p)_j^{(i)}+\delta(p)_j^{(i)})+((p)_{j-1}^{(i)}+\delta(p)_{j-1}^{(i)})}{2}\right)^2\\
&-\omega\lambda\left(\frac{((q)_j^{(i)}+\delta(q)_j^{(i)})+((q)_{j-1}^{(i)}+\delta(q)_{j-1}^{(i)})}{2}\right)^2\left(\frac{((q)_j^{(i)}+\delta(q)_j^{(i)})-((q)_{j-1}^{(i)}+\delta(q)_{j-1}^{(i)})}{h_j}\right)\\
&\pm\beta\left(\frac{((g)_j^{(i)}+\delta(g)_j^{(i)})+((g)_{j-1}^{(i)}+\delta(g)_{j-1}^{(i)})}{2}\right)\pm\delta\left(\frac{((s)_j^{(i)}+\delta(s)_j^{(i)})+((s)_{j-1}^{(i)}+\delta(s)_{j-1}^{(i)})}{2}\right)\\
&+K\left(\frac{((p)_j^{(i)}+\delta(p)_j^{(i)})+((p)_{j-1}^{(i)}+\delta(p)_{j-1}^{(i)})}{2}\right)=0,
\end{aligned} \tag{4.22}$$

$$\begin{aligned}
&\frac{1}{Pr}\left(1+\frac{4}{3}N\right)\left(\frac{((n)_j^{(i)}+\delta(n)_j^{(i)})-((n)_{j-1}^{(i)}+\delta(n)_{j-1}^{(i)})}{h_j}\right)+\left(\frac{((f)_j^{(i)}+\delta(f)_j^{(i)})+((f)_{j-1}^{(i)}+\delta(f)_{j-1}^{(i)})}{2}\right)\\
&\cdot\left(\frac{((n)_j^{(i)}+\delta(n)_j^{(i)})+((n)_{j-1}^{(i)}+\delta(n)_{j-1}^{(i)})}{2}\right)+Nb\left(\frac{((t)_j^{(i)}+\delta(t)_j^{(i)})+((t)_{j-1}^{(i)}+\delta(t)_{j-1}^{(i)})}{2}\right)\\
&\left(\frac{((n)_j^{(i)}+\delta(n)_j^{(i)})+((n)_{j-1}^{(i)}+\delta(n)_{j-1}^{(i)})}{2}\right)+Nt\left(\frac{((n)_j^{(i)}+\delta(n)_j^{(i)})+((n)_{j-1}^{(i)}+\delta(n)_{j-1}^{(i)})}{2}\right)^2\\
&+Ec\left(\frac{((q)_j^{(i)}+\delta(q)_j^{(i)})+((q)_{j-1}^{(i)}+\delta(q)_{j-1}^{(i)})}{2}\right)^2+Q\left(\frac{((g)_j^{(i)}+\delta(g)_j^{(i)})+((g)_{j-1}^{(i)}+\delta(g)_{j-1}^{(i)})}{2}\right)=0,
\end{aligned} \tag{4.23}$$

$$\frac{1}{Pr}\left(\frac{((t)_j^{(i)}+\delta(t)_j^{(i)})-((t)_{j-1}^{(i)}+\delta(t)_{j-1}^{(i)})}{h_j}\right)+Le\left(\frac{((f)_j^{(i)}+\delta(f)_j^{(i)})+((f)_{j-1}^{(i)}+\delta(f)_{j-1}^{(i)})}{2}\right)$$

$$\left(\frac{((t)_j^{(i)}+\delta(t)_j^{(i)})+((t)_{j-1}^{(i)}+\delta(t)_{j-1}^{(i)})}{2}\right)+\frac{Nt}{Nb}\left(\frac{((n)_j^{(i)}+\delta(n)_j^{(i)})-((n)_{j-1}^{(i)}+\delta(n)_{j-1}^{(i)})}{h_j}\right)$$
$$-R\left(\frac{((s)_j^{(i)}+\delta(s)_j^{(i)})+((s)_{j-1}^{(i)}+\delta(s)_{j-1}^{(i)})}{2}\right)=0, \tag{4.24}$$

$$(\delta(f)_j^{(i)}-\delta(f)_{j-1}^{(i)})-\frac{h}{2}(\delta(p)_j^{(i)}+\delta(p)_{j-1}^{(i)})=(r_1)_{j-\frac{1}{2}}, \tag{4.25}$$

$$(\delta(p)_j^{(i)}-\delta(p)_{j-1}^{(i)})-\frac{h}{2}(\delta(q)_j^{(i)})+(\delta(q)_{j-1}^{(i)})=(r_2)_{j-\frac{1}{2}}, \tag{4.26}$$

$$(\delta(g)_j^{(i)})-(\delta(g)_{j-1}^{(i)})-\frac{h}{2}(\delta(n)_j^{(i)})+(\delta(n)_{j-1}^{(i)})=(r_3)_{j-\frac{1}{2}}, \tag{4.27}$$

$$(\delta(s)_j^{(i)})-(\delta(s)_{j-1}^{(i)})-\frac{h}{2}(\delta(t)_j^{(i)})+(\delta(t)_{j-1}^{(i)})=(r_4)_{j-\frac{1}{2}}, \tag{4.28}$$

$$(1+\omega)\left(\frac{\delta(q)_j^{(i)}-\delta(q)_{j-1}^{(i)}}{h_j}\right)+\left(\frac{\delta(f)_j^{(i)}+\delta(f)_{j-1}^{(i)}}{2}\right)\left(\frac{\delta(q)_j^{(i)}+\delta(q)_{j-1}^{(i)}}{2}\right)-\left(\frac{\delta(p)_j^{(i)}+\delta(p)_{j-1}^{(i)}}{2}\right)^2$$
$$-\omega\lambda\left(\frac{\delta(q)_j^{(i)}+\delta(q)_{j-1}^{(i)}}{2}\right)^2\left(\frac{\delta(q)_j^{(i)}-\delta(q)_{j-1}^{(i)}}{h_j}\right)\pm\beta\left(\frac{\delta(g)_j^{(i)}+\delta(g)_{j-1}^{(i)}}{2}\right)$$
$$\pm\delta\left(\frac{\delta(s)_j^{(i)}+\delta(s)_{j-1}^{(i)}}{2}\right)+K\left(\frac{\delta(p)_j^{(i)}+\delta(p)_{j-1}^{(i)}}{2}\right)=(r_5)_{j-\frac{1}{2}}, \tag{4.29}$$

$$\frac{1}{Pr}\left(1+\frac{4}{3}N\right)\left(\frac{(\delta(n)_j^{(i)})-(\delta(n)_{j-1}^{(i)})}{h_j}\right)+\left(\frac{(\delta(f)_j^{(i)})+(\delta(f)_{j-1}^{(i)})}{2}\right)\left(\frac{(\delta(n)_j^{(i)})+(\delta(n)_{j-1}^{(i)})}{2}\right)$$
$$+Nb\left(\frac{(\delta(t)_j^{(i)})+(\delta(t)_{j-1}^{(i)})}{2}\right)\left(\frac{(\delta(n)_j^{(i)})+(\delta(n)_{j-1}^{(i)})}{2}\right)+Nt\left(\frac{(\delta(n)_j^{(i)})+(\delta(n)_{j-1}^{(i)})}{2}\right)^2$$
$$+Ec\left(\frac{\delta(q)_j^{(i)}+\delta(q)_{j-1}^{(i)}}{2}\right)^2+Q\left(\frac{\delta(g)_j^{(i)}+\delta(g)_{j-1}^{(i)}}{2}\right)=(r_6)_{j-\frac{1}{2}}, \tag{4.30}$$

$$\frac{1}{Pr}\left(\frac{\delta(t)_j^{(i)}-\delta(t)_{j-1}^{(i)}}{h_j}\right)+Le\left(\frac{\delta(f)_j^{(i)}+\delta(f)_{j-1}^{(i)}}{2}\right)\left(\frac{\delta(t)_j^{(i)}+\delta(t)_{j-1}^{(i)}}{2}\right)+\frac{Nt}{Nb}\left(\frac{\delta(n)_j^{(i)}-\delta(n)_{j-1}^{(i)}}{h_j}\right)$$
$$-R\left(\frac{\delta(s)_j^{(i)}+\delta(s)_{j-1}^{(i)}}{2}\right)=(r_7)_{j-\frac{1}{2}}, \tag{4.31}$$

where

$$(r_1)_{j-\frac{1}{2}}=-(f_j-f_{j-1})+\frac{h_j}{2}(p_j+p_{j-1}),$$
$$(r_2)_{j-\frac{1}{2}}=-(p_j-p_{j-1})+\frac{h_j}{2}(q_j+q_{j-1}),$$

$$(r_3)_{j-\frac{1}{2}} = -(g_j - g_{j-1}) + \frac{h_j}{2}(n_j + n_{j-1}),$$

$$(r_4)_{j-\frac{1}{2}} = -(s_j - s_{j-1}) + \frac{h_j}{2}(t_j + t_{j-1}),$$

$$(r_5)_{j-\frac{1}{2}} = -(1+\omega)(q_j - q_{j-1}) - h_j\left(\frac{f_j + f_{j-1}}{2}\right)\left(\frac{q_j + q_{j-1}}{2}\right) + h_j\left(\frac{p_j + p_{j-1}}{2}\right)^2 + \omega\lambda h_j\left(\frac{q_j + q_{j-1}}{2}\right)^2\left(\frac{q_j - q_{j-1}}{h_j}\right) \pm \beta h_j\left(\frac{g_j + g_{j-1}}{2}\right) \pm \delta h_j\left(\frac{s_j + s_{j-1}}{2}\right) - Kh_j\left(\frac{p_j + p_{j-1}}{2}\right),$$

$$(r_6)_{j-\frac{1}{2}} = -\frac{1}{Pr}\left(1 + \frac{4}{3}N\right)(n_j - n_{j-1}) - h_j\left(\frac{f_j + f_{j-1}}{2}\right)\left(\frac{n_j + n_{j-1}}{2}\right) - h_j Nb\left(\frac{t_j + t_{j-1}}{2}\right) \cdot \left(\frac{n_j + n_{j-1}}{2}\right) - h_j Nt\left(\frac{n_j + n_{j-1}}{2}\right)^2 - h_j Ec\left(\frac{q_j + q_{j-1}}{2}\right)^2 - h_j Q\left(\frac{g_j + g_{j-1}}{2}\right),$$

$$(r_7)_{j-\frac{1}{2}} = -\frac{1}{Pr}(t_j - t_{j-1}) - h_j Le\left(\frac{f_j + f_{j-1}}{2}\right)\left(\frac{t_j + t_{j-1}}{2}\right) - h_j\frac{Nt}{Nb}\left(\frac{n_j - n_{j-1}}{h_j}\right) + h_j R\left(\frac{s_j + s_{j-1}}{2}\right).$$

Upon substitution of $(i+1)$ boundary conditions are reduced into

$$\delta f_0 = 0, \quad \delta p_0 = 0,$$
$$\delta n_0 = 0, \quad \delta s_0 = 0,$$
$$\delta p_J = 0, \quad \delta g_J = 0, \quad \delta s_J = 0. \tag{4.32}$$

Block tridiagonal matrix is obtained from linearized difference equations (4.25)-(4.32) can be written as $A\delta = B$ where A is $J \times J$ block tridiagonal matrix and order of each block is $J+1 \times J+1$. Whereas δ and B are respectively column matrices of order $J \times 1$. The δ is determined by LU factorization, the $(i+1)$th iterate is obtained above mentioned Newton's method. Obtained solutions start with $\eta = 0$ with step size $h = 0.001$ for $o = \eta = \eta_\infty$ the convergence criterion has been taken for Iteration and stopped at $\left|\delta(q_0)^i\right| < \epsilon$ is satisfied for $\epsilon = 10^{-7}$.

5. Validation of Numerical Results

To know the exactness of our results we compare with previous study with a specific case the acquired numerical results are checked and verified for $\omega = \lambda = \beta = \delta = = k_1 = N = Nb = Nt = Ec = Q = Le = K = 0$ and $Bi \to \infty$ we are sure about the accuracy of our obtained in geometrically.

Table 1

$-\theta'(0)$			
Pr	Present study	Validation with Malik *et al.* [30]	Validation with Rashmi *et al.* [33]
0.7	0.8646285	0.86461923	0.862548
2.0	0.9113685	0.91135769	0.91136
3.0	1.89540327	1.89540340	1.89540

6. Results and Discussions

In this part, all of the numerical results from the figures are displayed visually to discuss the many resultant parameters encountered in the current study. The Keller-Box technique is efficient and impressive enough for use in dealing with fluid flow difficulties.

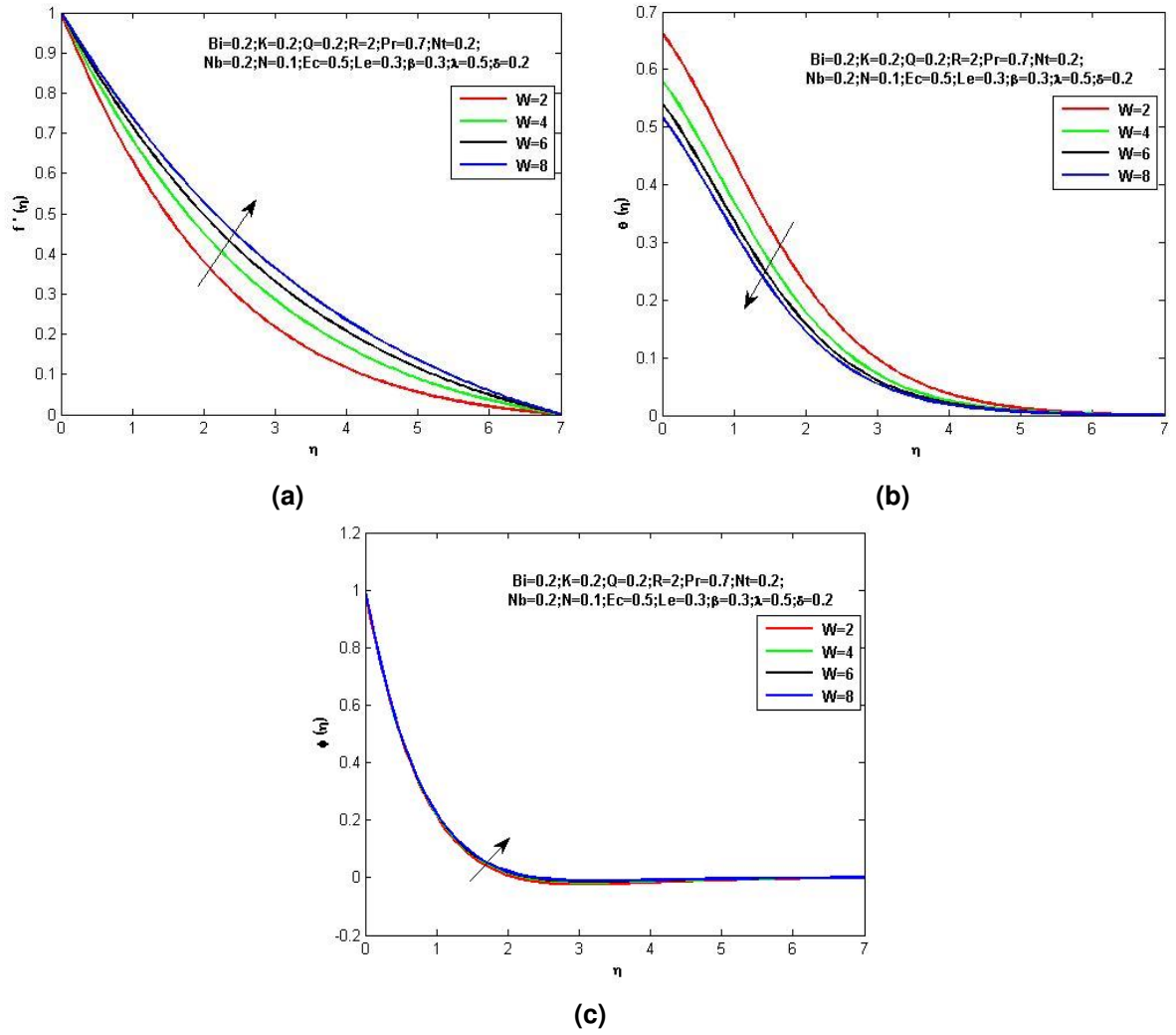

Figure 1

Figure 1(a)-1(c) depict the distribution of velocity, temperature, and concentration of the fluid with raising of Eyring-Powell fluid parameter ω. From Figures it is observed that as Eyring-Powell fluid parameter ω increases the momentum boundary layer thickness, and concentration boundary layer thickness are increasing whereas the thermal boundary layer thickness is decreasing, this is all only the cause of Eyring-Power fluids are share thinning fluids the velocity gets high at the share rate increases.

Biot number is characterizing the heat transfer resistance inside a solid body. Biot number is the ratio of internal conductive resistance to external convective resistance it is used determine lumped heat analysis temperature gradients within the particle should be considered in order to correctly predict the heat transfer rate to the surrounding fluid. From Figures 2(a)-2(c) it is depict that Biot number remarkably shown the power of convective heating. Layer Biot number

implicit stronger convective heating to which velocity and temperature rises gradually with increasing of Biot number. While concentration boundary layer thickness is decreasing.

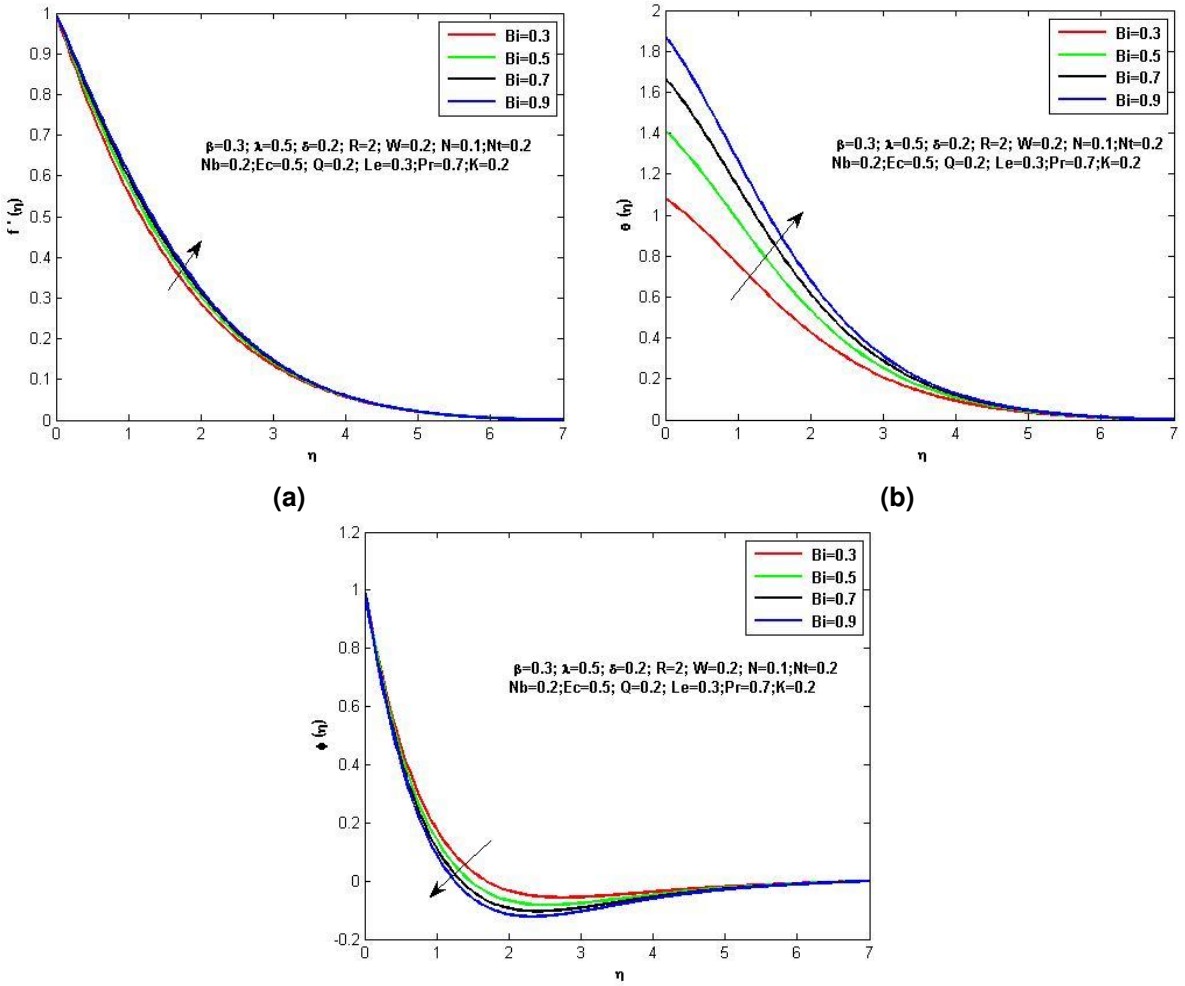

Figure 2

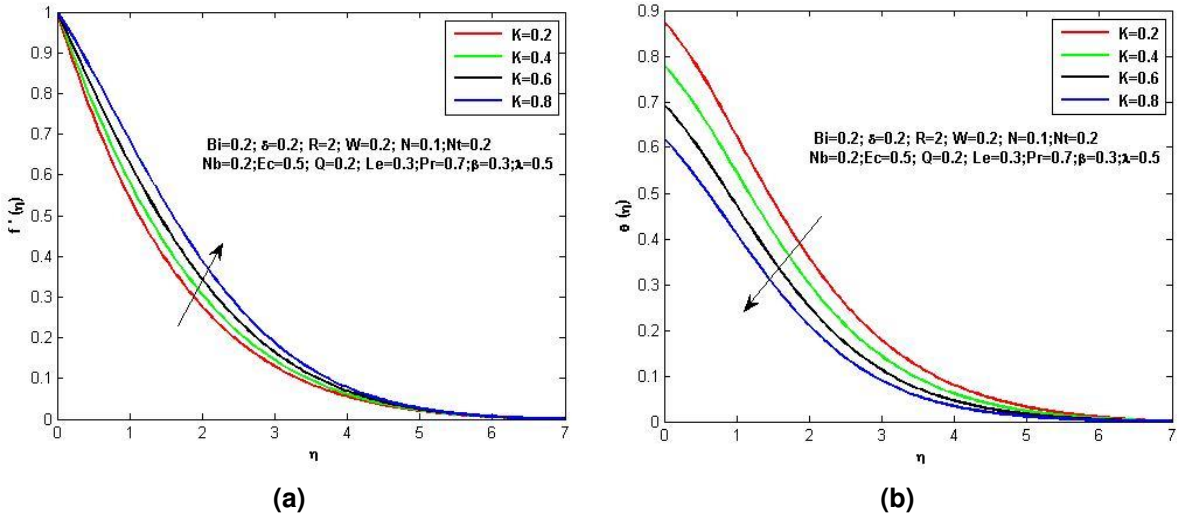

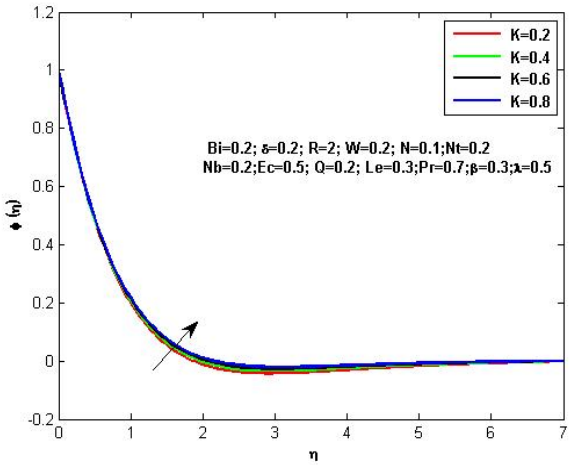

(c)

Figure 3

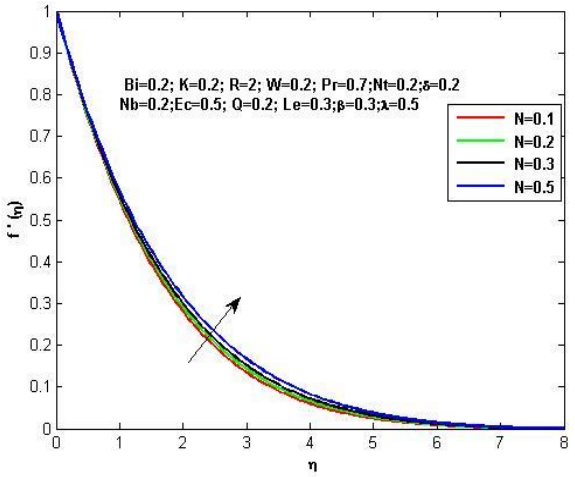

(a)

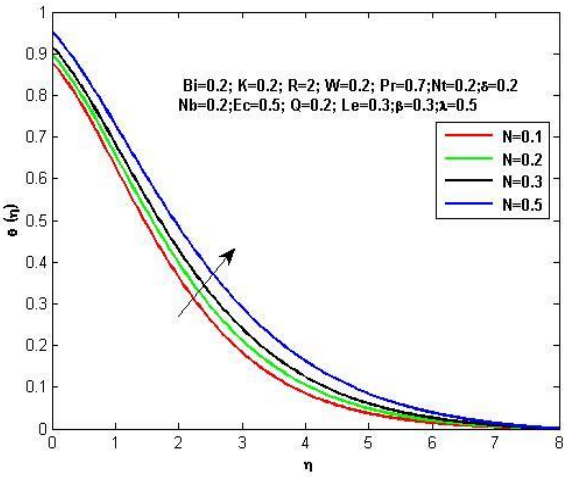

(b)

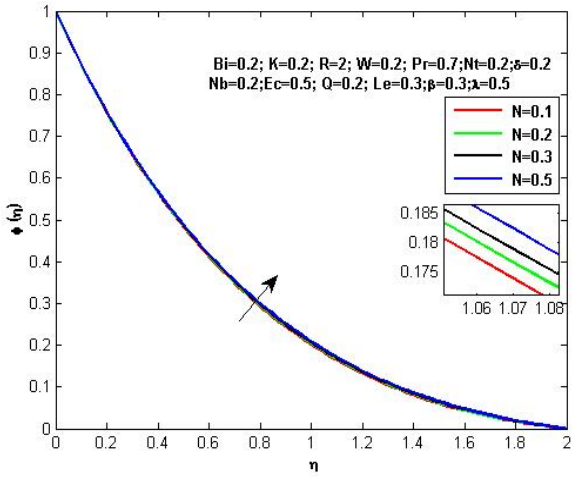

(c)

Figure 4

It is evident that the porosity is a significant parameter for characterization of material microstructures. It corresponds to the volume of pores that can contain fluid related to the volume of the material. Because of this nature Figure 3(a)-3(b) shows that as the porosity parameter K increases so as the velocity, concentration profiles of the fluid increases but the thermal boundary layer thickness is decreases.

It is well known that increasing in radiation parameter enhances the energy transport inside the fluid, consequently rate of heat transfer at the surface increased. So from Figures 4(a)-4(c) it is depict that the boundary layer thickness of momentum, thermal, and concentration of the fluid will increase gradually.

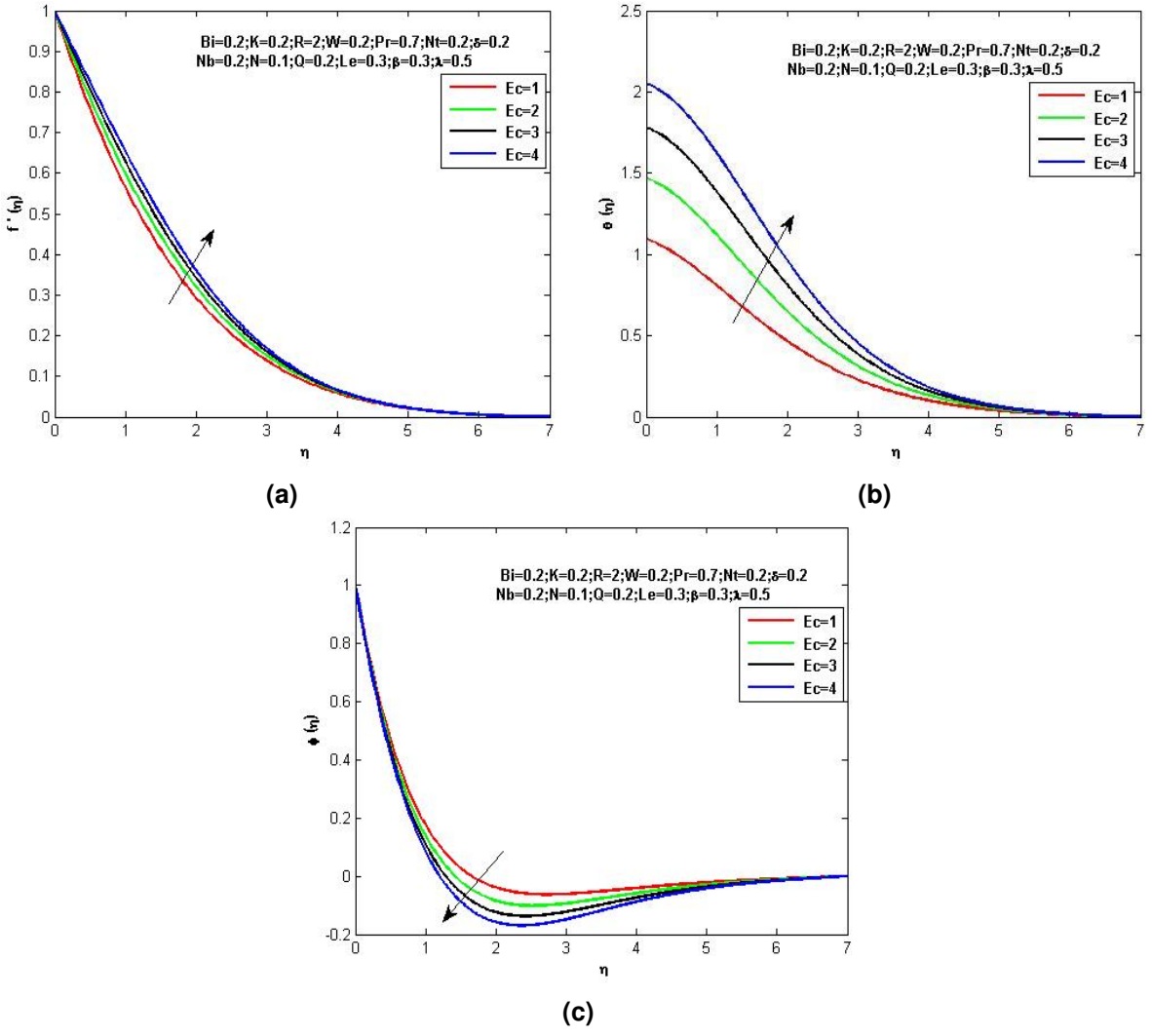

Figure 5

The Eckert number expresses the conversion of kinetic energy into internal energy by work done against the viscous fluid stress. As a result it is observed that the thermal and momentum boundary layer becomes thinner with large value of Eckert number. So that the velocity, and temperature profiles of the fluid is increasing, while the boundary layer thickness of the concentration of the fluid is reduces gradually which are shown in Figure 5(a)-5(c).

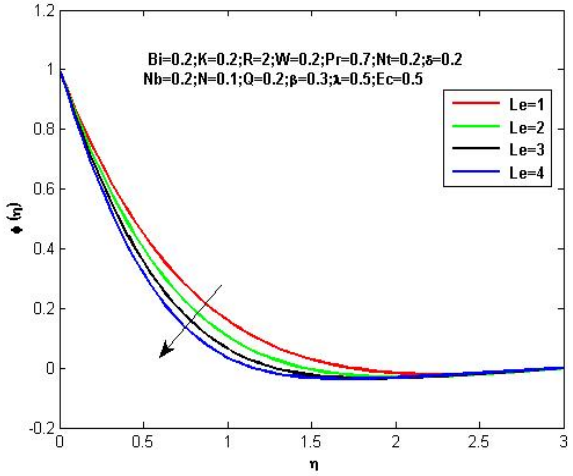

Figure 6

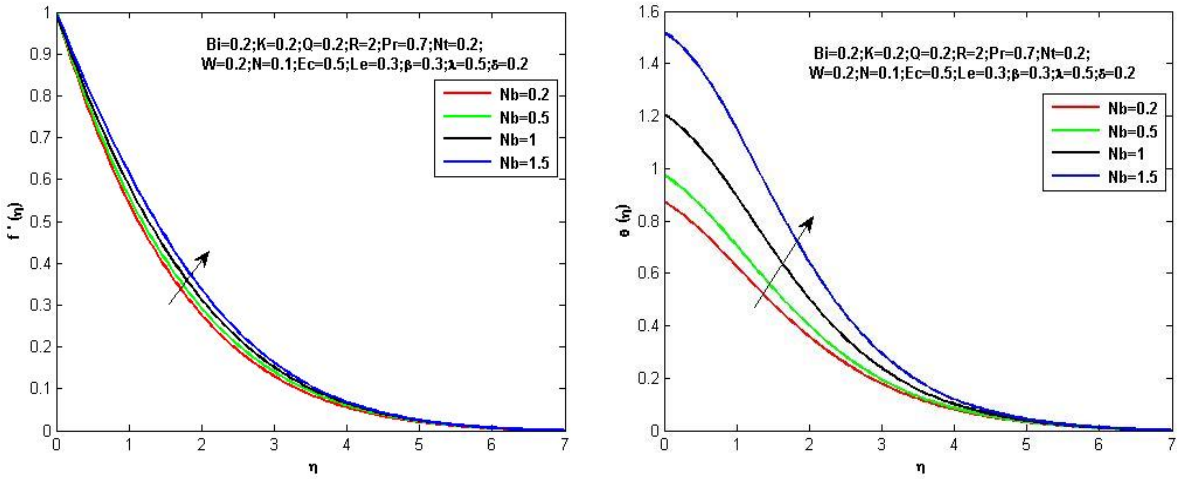

(a) **(b)**

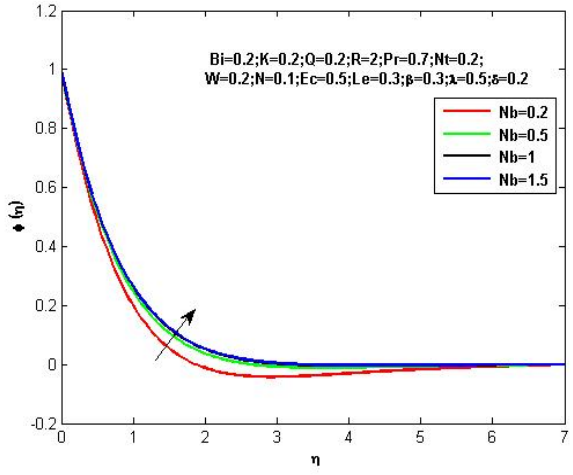

(c)

Figure 7

Effect of Lewis number is analysed through Figure 6 nanoparticle concentration is a decreasing function of *Le*. Since stronger Lewis number intimates a weaker Brownian diffusion coefficient which result relatively small penetration depth for the concentration boundary layer, i.e., with an increasing value of Lewis number the concentration profile is decreasing.

Large Brownian motion parameter *Nb* causes enlargement of the liquid temperature this ensures on the reason of slow expanse in nanoparticles measurement with *Nb*. Because of this nature from Figures 7(a)-7(b) it can revealed that as an increasing in the Brownian motion parameter *Nb*, boundary layer thickness of the momentum, temperature, and concentration of the fluid is thinner hence the velocity, temperature, and nanoparticle volume concentration profiles are increasing.

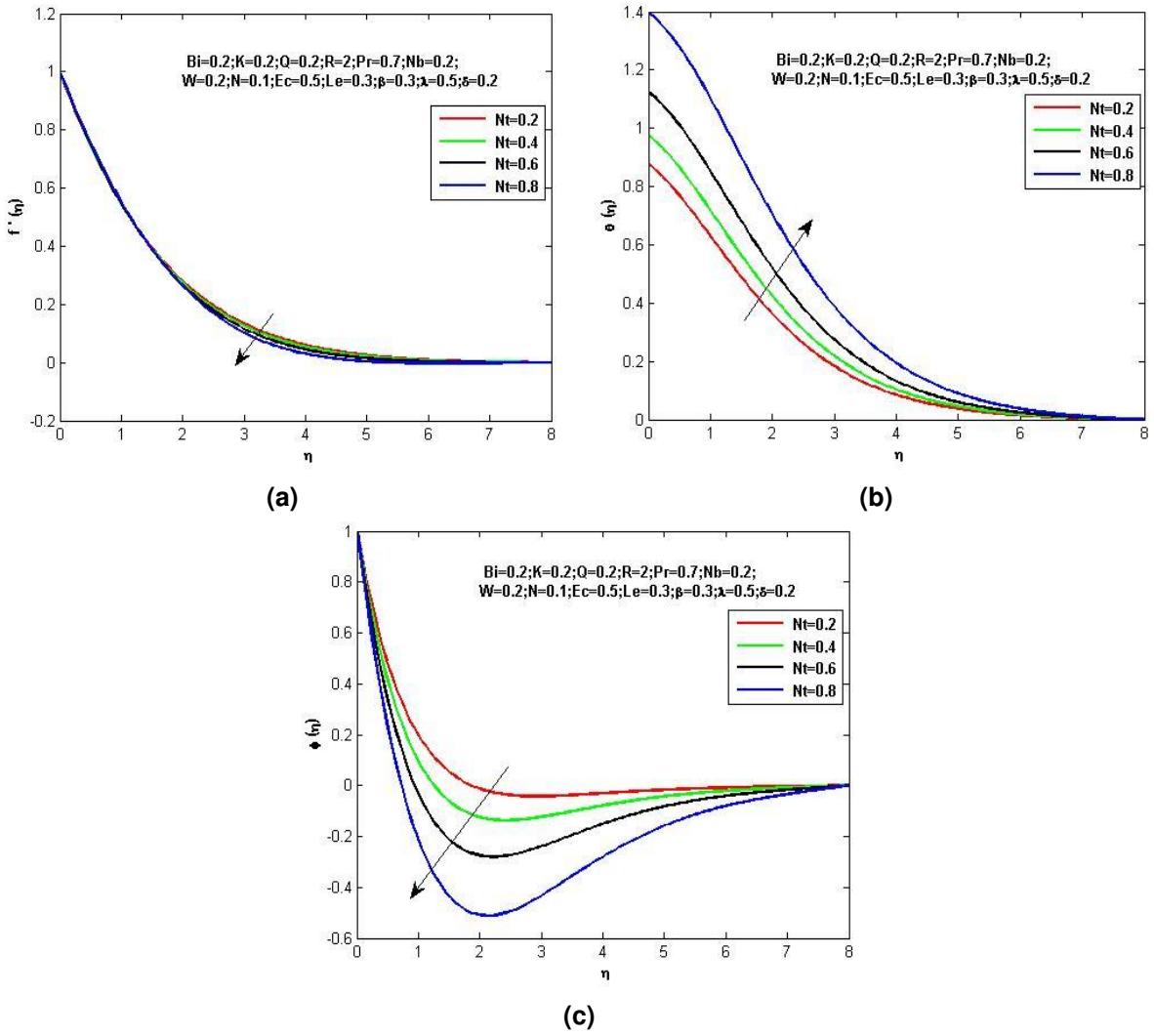

Figure 8

Figures 8(a)-8(c) revels that effect of Thermophoresis parameter *Nt* on velocity, temperature and nanoparticle volume concentration profiles. Thermophoresis mechanism is associated with elements averaged Brownian motion under a steady thermal gradient. This phenomenon leads to disperse the nanoparticles from the hot surface to the ambient fluid, since the nanometer

size particles experience resistance from heated surface. Therefore the thermophoretic force permits nanoparticles to import heat from the surface to the moving fluids consequently thicken concentration boundary layer hence the velocity, and nanoparticles concentration profile decreases, and the boundary layer thickness of the temperature is thinner as an increasing value of the thermophoretic parameter Nt.

7. Conclusions

This work looks at the physical characteristics of Eyring-Powell Casson nanofluid on a stretched surface. The flow control issue's numerical solution The characteristics of non-Newtonian Casson nanofluid mixed convection boundary layer flow through porous media have been finished and characterised for changing physical parameter values. The following are the study's key findings:

- As the Eyring-Powell fluid parameter increases in both flow circumstances, the velocity profile and momentum boundary layer thickness increase.
- the curves of other velocity profile for various values β and at fixed values of other parameters. The gradual increasing in assisting flow and slow down the in the opposing flow with various values of β.
- the curves of f' for difference of mass buoyancy parameter δ are presented at specific values of other parameters and for opposing and assisting flows the velocity profile can be seen as for increase and decreasing respectively .
- Recorded for higher values on Eyring-Powell fluid parameter ω and heat of fluid rises for opposing assisting flow.
- Temperature rises gradually with increasing of Biot number rises for opposing assisting flow.
- Also observed that temperature falls down very significantly with increasing values of Prandtl number. In both cases of opposing and assisting flows.
- The concentration contour increases with increase in Eyring-Powell fluid parameter ω rises for opposing assisting flow.
- The concentration contours differ that Brownian motion parameter Nb and thermophoresis parameter Nt. The concentration and the solutal buoyancy layer diameter within increasing in the thermophoresis parameter, duration of the decrease in the concentration and solutal buoyancy layer diameter is seen in that increasing rates of the Brownian motion parameter.
- The concentration buoyancy layer thickness decreases with increase in Le for both cases which is observed

Competing Interests

The authors declare that they have no competing interests.

Authors' Contributions

All the authors contributed significantly in writing this article. The authors read and approved the final manuscript.

References

[1] M. H. Abolbashari, N. Freidoonimehr, F. Nazari and M. M. Rashidi, Analytical modeling of entropy generation for Casson nano-fluid flow induced by a stretching surface, *Advanced Powder Technology* **26**(2) (2015), 542 – 552, DOI: 10.1016/j.apt.2015.01.003.

[2] F. Ahmad, M. Nazeer, M. Saeed, A. Saleem and W. Ali, Heat and mass transfer of temperature-dependent viscosity models in a pipe: effects of thermal radiation and heat generation, *Zeitschrift für Naturforschung A* **75**(3) (2020), 225 – 239, DOI: 10.1515/zna-2019-0332.

[3] K. Ahmad, Z. Hanouf and A. Ishak, MHD Casson nanofluid flow past a wedge with Newtonian heating, *The European Physical Journal Plus* **132** (2017), Article number: 87, DOI: 10.1140/epjp/i2017-11356-5.

[4] A. Al-Mudhaf and A. J. Chamkha, Similarity solutions for MHD thermosolutal Marangoni convection over a flat surface in the presence of heat generation or absorption effects, *Heat and Mass Transfer* **42** (2005), 112 – 121, DOI: 10.1007/s00231-004-0611-8.

[5] H. A. Attia, Investigation of non-Newtonian micropolar fluid flow with uniform suction/blowing and heat generation, *Turkish Journal of Engineering and Environmental Sciences* **30**(6) (2006), 359 – 365.

[6] A. J. Chamkha, On laminar hydromagnetic mixed convection flow in a vertical channel with symmetric and asymmetric wall heating conditions, *International Journal of Heat and Mass Transfer* **45**(12) (2002), 2509 – 2525, DOI: 10.1016/S0017-9310(01)00342-8.

[7] A. J. Chamkha, T. Groşan and I. Pop, Fully developed free convection of a micropolar fluid in a vertical channel, *International Communications in Heat and Mass Transfer* **29**(8) (2002), 1119 – 1127, DOI: 10.1016/S0735-1933(02)00440-2.

[8] A. J. Chamkha and A.-R. A. Khaled, Hydromagnetic combined heat and mass transfer by natural convection from a permeable surface embedded in a fluid-saturated porous medium, *International Journal of Numerical Methods for Heat & Fluid Flow* **10**(5) (2000), 455 – 477, DOI: 10.1108/09615530010338097.

[9] A. S. Dogonchi and D. D. Ganji, Investigation of MHD nanofluid flow and heat transfer in a stretching/shrinking convergent/divergent channel considering thermal radiation, *Journal of Molecular Liquids* **220** (2016), 592 – 603, DOI: 10.1016/j.molliq.2016.05.022.

[10] M. A. El-Aziz and A. A. Afify, influences of slip velocity and induced magnetic field on MHD stagnation-point flow and heat transfer of casson fluid over a stretching sheet, *Mathematical Problems in Engineering* **2018** (2018), Article ID 9402836, 11 pages, DOI: 10.1155/2018/9402836.

[11] N. T. M. Eldabe and S. N. Sallam, Non-Darcy Couette flow through a porous medium of magnetohydro-dynamic visco-elastic fluid with heat and mass transfer, *Canadian Journal of Physics* **83**(12) (2005), 1243 – 1265, DOI: 10.1139/P05-056.

[12] N. T. M. Eldabe, G. M. Moatimid and H. S. Ali, Magnetohydrodynamic flow of non-Newtonian visco-elastic fluid through a porous medium near an accelerated plate, *Canadian Journal of Physics* **81**(11) (2003), 1249 – 1269, DOI: 10.1139/p03-092.

[13] E. O. Fatunmbi and A. T. Adeosun, Nonlinear radiative Eyring-Powell nanofluid flow along a vertical Riga plate with exponential varying viscosity and chemical reaction, *International Communications in Heat and Mass Transfer* **119** (2020), 104913, DOI: 10.1016/j.icheatmasstransfer.2020.104913.

[14] R. S. R. Gorla, A. J. Chamkha and A. M. Rashad, Mixed convective boundary layer flow over a vertical wedge embedded in a porous medium saturated with a nanofluid: Natural convection dominated regime, *Nanoscale Research Letters* **6** (2011), 207, DOI: 10.1186/1556-276X-6-207.

[15] M. Hameed and S. Nadeem, Unsteady MHD flow of a non-Newtonian fluid on a porous plate, *Journal of Mathematical Analysis and Applications* **325**(1) (2007), 724 – 733, DOI: 10.1016/j.jmaa.2006.02.002.

[16] T. Hayat, S. A. Shehzad and A. Alsaedi, Soret and Dufour effects on magnetohydrodynamic (MHD) flow of Casson fluid, *Applied Mathematics and Mechanics* **33** (2012), 1301 – 1312, DOI: 10.1007/s10483-012-1623-6.

[17] T. Hussain, S. A. Shehzad, A. Alsaedi, T. Hayat and M. Ramzan, Flow of Casson nanofluid with viscous dissipation and convective conditions: A mathematical model, *Journal of Central South University* **22** (2015), 1132 – 1140, DOI: 10.1007/s11771-015-2625-4.

[18] A. Hussanan, M. Z. Salleh, I. Khan and R. M. Tahar, Heat transfer in magnetohydrodynamic flow of a Casson fluid with porous medium and Newtonian heating, *Journal of Nanofluids* **6**(4) (2017), 784 – 793, DOI: 10.1166/jon.2017.1359.

[19] A. Hussanan, M. Z. Salleh, I. Khan and R. M. Tahar, Unsteady heat transfer flow of a casson fluid with newtonian heating and thermal radiation, *Jurnal Teknologi* **78** (2016), 1–7, DOI: 10.11113/jt.v78.8264.

[20] S. M. Ibrahim, G. Lorenzini, P. V. Kumar and C. S. K. Raju, Influence of chemical reaction and heat source on dissipative MHD mixed convection flow of a Casson nanofluid over a nonlinear permeable stretching sheet, *International Journal of Heat and Mass Transfer* **111** (2017), 346 – 355, DOI: 10.1016/j.ijheatmasstransfer.2017.03.097.

[21] T. Javed, M. Faisal and I. Ahmad, Dynamisms of solar radiation and prescribed heat sources on bidirectional flow of magnetized Eyring-Powell nanofluid, *Case Studies in Thermal Engineering* **21** (2020), 100689, DOI: 10.1016/j.csite.2020.100689.

[22] M. Keimanesh, M. M. Rashidi, A. J. Chamkha and R. Jafari, Study of a third grade non-Newtonian fluid flow between two parallel plates using the multi-step differential transform method, *Computers & Mathematics with Applications* **62**(8) (2011), 2871 – 2891, DOI: 10.1016/j.camwa.2011.07.054.

[23] H. B. Keller, A new difference scheme for parabolic problems, in: *Numerical Solution of Partial Differential Equations–II*, Proceedings of the Second Symposium on the Numerical Solution of Partial Differential Equations, SYNSPADE 1970, University of Maryland, College Park, Maryland, May 11-15, 1970, 327 – 350 (1971), DOI: 10.1016/B978-0-12-358502-8.50014-1.

[24] A. A. Khan, F. Zaib and A. Zaman, Effects of entropy generation on Powell Eyring fluid in a porous channel, *Journal of the Brazilian Society of Mechanical Sciences and Engineering* **39** (2017), 5027 – 5036, DOI: 10.1007/s40430-017-0881-y.

[25] M. R. Krishnamurthy, B. C. Prasannakumara, B. J. Gireesha and R. S. R. Gorla, Effect of chemical reaction on MHD boundary layer flow and melting heat transfer of Williamson nanofluid in porous medium, *Engineering Science and Technology, an International Journal* **19**(1) (2016), 53 – 61, DOI: 10.1016/j.jestch.2015.06.010.

[26] B. Krishnendu, H. Tasawar and A. Ahmed, Analytic solution for magnetohydrodynamic boundary layer flow of Casson fluid over a stretching/shrinking sheet with wall mass transfer, *Chinese Physics B* **22**(2) (2013), 024702, DOI: 10.1088/1674-1056/22/2/024702.

[27] P. S. Kumar and K. Gangadhar, Effect of chemical reaction on slip flow of MHD Casson fluid over a stretching sheet with heat and mass transfer, *Advances in Applied Science Research* **6**(8) (2015), 205 – 223.

[28] F. Mabood, S. Shateyi, M. M. Rashidi, E. Momoniat and N. Freidoonimehr, MHD stagnation point flow heat and mass transfer of nanofluids in porous medium with radiation, viscous dissipation and chemical reaction, *Advanced Powder Technology* **27**(2) (2016), 742 – 749, DOI: 10.1016/j.apt.2016.02.033.

[29] M. Y. Malik, I. Khan, A. Hussain and T. Salahuddin, Mixed convection flow of MHD Eyring-Powell nanofluid over a stretching sheet: A numerical study, *AIP Advances* **5** (2015), 117118, DOI: 10.1063/1.4935639.

[30] M. Y. Malik, T. Salahuddin, A. Hussain and S. Bilal, MHD flow of tangent hyperbolic fluid over a stretching cylinder: Using Keller-Box method, *Journal of Magnetism and Magnetic Materials* **395** (2015), 271 – 276, DOI: 10.1016/j.jmmm.2015.07.097.

[31] M. Nazeer, M. I. Khan, M. U. Rafiq and N. B. Khan, Numerical and scale analysis of Eyring-Powell nanofluid towards a magnetized stretched Riga surface with entropy generation and internal resistance, *International Communications in Heat and Mass Transfer* **119** (2020), 104968, DOI: 10.1016/j.icheatmasstransfer.2020.104968.

[32] S. Pramanik, Casson fluid flow and heat transfer past an exponentially porous stretching surface in presence of thermal radiation, *Ain Shams Engineering Journal* **5**(1) (2014), 205 – 212, DOI: 10.1016/j.asej.2013.05.003.

[33] J. Rahimi, D. D. Ganji, M. Khaki and K. Hosseinzadeh, Solution of the boundary layer flow of an Eyring-Powell non-Newtonian fluid over a linear stretching sheet by collocation method, *Alexandria Engineering Journal* **56**(4) (2017), 621 – 627, DOI: 10.1016/j.aej.2016.11.006.

[34] C. S. K. Raju, N. Sandeep, V. Sugunamma, M. J. Babu and J. V. R. Reddy, Heat and mass transfer in magnetohydrodynamic Casson fluid over an exponentially permeable stretching surface, *Engineering Science and Technology, an International Journal* **19**(1) (2016), 45 – 52, DOI: 10.1016/j.jestch.2015.05.010.

[35] G. K. Ramesh, B. C. Prasannakumara, B. J. Gireesha and M. M. Rashidi, Casson fluid flow near the stagnation point over a stretching sheet with variable thickness and radiation, *Journal of Applied Fluid Mechanics* **9**(3) (2016), 1115 – 1022, DOI: 10.18869/acadpub.jafm.68.228.24584.

[36] K. U. Rehman, A. A. Khan, M. Y. Malik and O. D. Makinde, Thermophysical aspects of stagnation point magnetonanofluid flow yields by an inclined stretching cylindrical surface: a non-Newtonian fluid model, *Journal of the Brazilian Society of Mechanical Sciences and Engineering* **39** (2017), 3669 – 3682, DOI: 10.1007/s40430-017-0860-3.

[37] G. Sarojamma and K. Vendabai, Boundary layer flow of a Casson nanofluid past a vertical exponentially stretching cylinder in the presence of a transverse magnetic field with internal heat generation/absorption, *International Scholarly and Scientific Research & Innovation* **9**(1) (2015), 138 – 143.

[38] M. Shojaeian and A. Koşar, Convective heat transfer and entropy generation analysis on Newtonian and non-Newtonian fluid flows between parallel-plates under slip boundary conditions, *International Journal of Heat and Mass Transfer* **70** (2014), 664 – 673, DOI: 10.1016/j.ijheatmasstransfer.2013.11.020.

[39] H. S. Takhar, A. J. Chamkha and G. Nath, MHD flow over a moving plate in a rotating fluid with magnetic field, Hall currents and free stream velocity, *International Journal of Engineering Science* **40**(13) (2002), 1511 – 1527, DOI: 10.1016/S0020-7225(02)00016-2.

[40] J. C. Umavathi, A. J. Chamkha, A. Mateen and A. Al-Mudhaf, Unsteady two-fluid flow and heat transfer in a horizontal channel, *Heat and Mass Transfer* **42** (2005), 81 – 90, DOI: 10.1007/s00231-004-0565-x.

[41] N. Yilmaz, A. S. Bakhtiyarov and R. N. Ibragimov, Experimental investigation of Newtonian and non-Newtonian fluid flows in porous media, *Mechanics Research Communications* **36**(5) (2009), 638 – 641, DOI: 10.1016/j.mechrescom.2009.01.012.